Accepted Manuscript

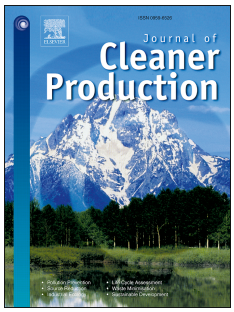

Optimal feed flow sequence for multi-effect distillation system integrated with supercritical carbon dioxide Brayton cycle for seawater desalination

Prashant Sharan, Ty Neises, Craig Turchi

PII: S0959-6526(18)31658-5

DOI: 10.1016/j.jclepro.2018.06.009

Reference: JCLP 13155

To appear in: *Journal of Cleaner Production*

Received Date: 22 February 2018

Revised Date: 30 April 2018

Accepted Date: 2 June 2018

Please cite this article as: Sharan P, Neises T, Turchi C, Optimal feed flow sequence for multi-effect distillation system integrated with supercritical carbon dioxide Brayton cycle for seawater desalination, *Journal of Cleaner Production* (2018), doi: 10.1016/j.jclepro.2018.06.009.

This is a PDF file of an unedited manuscript that has been accepted for publication. As a service to our customers we are providing this early version of the manuscript. The manuscript will undergo copyediting, typesetting, and review of the resulting proof before it is published in its final form. Please note that during the production process errors may be discovered which could affect the content, and all legal disclaimers that apply to the journal pertain.

ACCEPTED MANUSCRIPT

Optimal Feed Flow Sequence for Multi-Effect Distillation System Integrated with Supercritical Carbon Dioxide Brayton Cycle for Seawater Desalination

Prashant Sharan,*

Ty Neises,

and

Craig Turchi

Buildings & Thermal Science Center, National Renewable Energy Laboratory, Golden 80401, Colorado USA

** Corresponding author: Tel:+1-303-275-3067; E-mail: prashant.sharan@nrel.gov*

ACCEPTED MANUSCRIPT

ACCEPTED MANUSCRIPT

Word Count:8569

Abstract

Multi-effect distillation is often integrated with a Rankine power cycle for cogeneration (simultaneous production of power and desalinated water). Such integration increases the condenser operating pressure for the Rankine cycle (and increases the heat-rejection temperature) to produce desalinated water, resulting in decreased power-plant efficiency. The supercritical carbon dioxide Brayton cycle has a higher efficiency compared to the Rankine cycle. The waste heat rejected from supercritical carbon dioxide Brayton cycle is at sufficiently hot temperature to have feasible energy integration with multi-effect distillation system. The paper introduces the novel concept of cogeneration without being a parasitic load to the power cycle. For the illustrative example considered, integrating 4-effect distillation system with a 115 MW_e power plant can produce 3041 m^3 of distillate per day at 1.06 $/$m^3$, at a constant power plant efficiency of 49.2%. The pattern in which feed enters the desalination system often dictates its energy consumption. The two most commonly used feed configurations for multi-effect distillation system are parallel/cross feed and forward feed. With steam as a heat source (i.e., a latent heat source), parallel/cross feed is the most energy-efficient feed configuration. The other objective of this paper is to identify the optimal feed flow configuration for multi-effect distillation system integrated with a supercritical carbon dioxide power cycle (i.e., a sensible heat source). For the simplified network, forward feed is the best feed configuration, which yields a 7.5% increase in distillate production at 2.6% reduced distillate cost. Additionally, different methods for reducing the brine discharge are studied, which can help to achieve zero liquid discharge. Result show increasing the maximum brine concentration gives superior results compared to brine recycling. The system modelling is done using the principle of process integration, and an analytical methodology for cogeneration is derived.

Key word

Multi-effect distillation, Supercritical carbon dioxide Brayton cycle, Brine recycling, Process integration

ACCEPTED MANUSCRIPT

Nomenclature

A	Specific area requirement
B	brine flow rate (kg/s)
C	cost ($)
C_p	Specific heat (kJ/kg/°C)
CU	cold utility (MW)
D	Net distillate produced (kg/s)
E	amount by which the effect is shifted away from pinch (kW)
F	feed flow rate (kg/s)
h	enthalpy (kJ/kg)
H	vapor enthalpy (kJ/kg)
HU	hot utility (kW)
K	total number of effects
M	mass of steam
n	effect under consideration
NEA	Non-equilibrium allowance (°C)
ΔT	temperature driving force (°C)
T	temperature (°C)
U	heat-transfer coefficient (W/m^2K)
V	vapor flow rate (kg/s)
W	demineralized water flow rate (kg/s)
X	brine concentration (ppm)

Greek Letter

λ	latent heat of vaporization (kJ/kg)
Δ	change

Subscript

cond	condensate
evap	evaporator
f	feed

ACCEPTED MANUSCRIPT

s	steam
sat	saturation
w	*water*

Subscript

new	new/updated value

Abbreviations

BPR	Boiling point rise
MED	Multi-effect distillation
PCHE	Printed-circuit heat exchanger
PH	Feed preheater
PFHE	Plate-and-frame heat exchanger
sCO_2	Supercritical carbon dioxide
TVC	Thermo-vapor compressor

ACCEPTED MANUSCRIPT

1. Introduction

The supercritical carbon dioxide (sCO_2) Brayton cycle offers the potential for simpler power block design and higher power-cycle efficiency (Conboy and Fuller, 2012). The sCO_2 Brayton cycle is being explored as a replacement to the ubiquitous steam-Rankine power cycle for several applications, including: concentrating solar power (Bauer et al., 2016), nuclear reactors (Dostal, 2004), waste-heat recovery (Lehar and Michelassi, 2013), geothermal applications (Sabau et al., 2011), and thermal energy storage (Jaroslav et al., 2011). Recently, the U.S. department of energy (DOE) awarded $80 million for development of a 10 MW sCO_2 Brayton cycle pilot plant (DOE, 2016).

The sCO_2 cycle is a closed-loop Brayton cycle that operates between a low pressure near the CO_2 critical point (7.37 MPa) and a high pressure that is typically around 25 MPa (Brun et al., 2017). Because CO_2 is very dense near the critical point, the cycle requires relatively low compressor work. Lower-compression work and higher operating temperature gives the sCO_2 cycle the potential to reach higher thermodynamic efficiencies than conventional steam-Rankine cycles (Ahn et al., 2015). Fleming et al. (2013) showed that for temperatures greater than 425°C, the sCO_2 Brayton cycle has a higher efficiency than the Rankine cycle; and for temperatures greater that 550°C, the sCO_2 cycle is more efficient than supercritical and superheated steam cycles (Hinze et al., 2017).

Furthermore, because the CO_2 remains at high densities, the cycle requires small, compact turbomachinery, which may result in lower capital cost (Turchi et al., 2012) and reduce operation and maintenance costs relative to the steam-Rankine cycle (Lee and Kim, 2014). Finally, researchers have found that because the cycle rejects its heat over a temperature range, it is better suited to dry-cooling requirements in arid regions (Hinze et al., 2017). Of the various sCO_2 cycle configuration proposed (recuperative, isothermal compression, re-heating, recompression, etc.), recompression cycle is most researched one, because of its higher efficiency and slight modification compared to simple cycle (Tse and Neises, 2016).

Multi-effect distillation (MED) is a commonly used thermal desalination system for production of freshwater from seawater. MED has several evaporators (“effects”) placed in

series, and an external heat source, generally steam, is used to heat the first effect of the MED train. Due to addition of heat in the first effect, the feed seawater gets evaporated to produce a salt-free vapor and partially concentrated brine. The vapor produced acts as a heat source for the second effect of the MED, where additional vapor is produced. This process continues until the last effect of the MED system. The vapor produced from each effect after condensing is stored as distillate (freshwater).

For cogeneration (simultaneous production of power and distillate) MED is often integrated with a steam-Rankine power cycle, where steam is extracted from the turbine to provide the heat source. Integrating MED with the power cycle helps in reduction of overall fuel energy consumption (Ihm et al., 2016). To have a feasible energy integration, the steam leaving the turbine should be sufficiently hot to act as a heat source for the MED. This extraction reduces the net power generation from the turbine, leading to reduced efficiency of the steam-Rankine cycle. Ortega-Delgado et al. (2016) showed that for producing 4474 m^3/d of distillate, the power cycle efficiency decreased by 6.1% point and the steam left the turbine at 70°C. Hence, the MED desalination system is a parasitic load for the power plant.

In contrast, the sCO_2 entering the heat-rejection stage of the Brayton cycle is sufficiently hot to drive an MED system, and hence, this heat could be tapped without being a parasitic load for the power plant. The sCO_2 Brayton cycle rejects its heat in the form of sensible heat, compared to isothermal condensation for the steam-Rankine cycle. The temperature of sCO_2 entering the cooler is quite hot (>80°C) and needs to be cooled to 32°C. That is, the temperature of sCO_2 is hot enough to drive a MED system for production of freshwater.

Recently researchers have investigated integration of MED with sCO_2 power cycle (Kouta et al., 2017; Lee et al., 2017). Kouta et al. (2017) integrated solar driven sCO_2 Brayton cycle with MED-TVC system, where TVC is the thermo-vapor compressor. TVC is used for increasing the energy efficiency of the MED system (Sharan and Bandyopadhyay, 2016a). The steam generated via solar collector loop at 224°C, acted as a heat source for the MED-TVC system and the waste heat from the sCO_2 cycle was used for feed pre-heating. Lee et al. (2017) on the other hand used the 3.3% of sCO_2 leaving the turbine at 240°C to act as a heat source for the 400 MW_{th} MED. It may be noted that these studies did not used the waste heat from sCO_2 power cycle as a primary heat source for distillate generation.

MED energy consumption is a function of feedwater flow in the system. The two most commonly used feed configurations for MED systems are parallel/cross feed and forward feed. In parallel/cross feed, feedwater enters each MED effect with almost equal flowrate, and the brine attains a maximum concentration at the end of each effect. In forward feed, the feed seawater enters the MED from the first effect. The feed gets partially concentrated in the first effect and enters the second effect where it is further concentrated. In forward feed, brine attains a maximum concentration at the end of the last effect. With steam as an external heating source for MED, parallel/cross feed MED is more energy-efficient compared to forward feed (Sharan and Bandyopadhyay, 2016b). Various studies on integration of MED with low-temperature sensible heat source can be found in literature (Christ et al., 2015; Rahimi et al., 2014; Wang and Lior, 2011). Wang and Lior, (2011) developed model for MED integrated with low-temperature heat source, and to further enhance the energy recovery they proposed boosted MED concept. Christ et al. (2015) showed boosted MED gives 20% higher distillate production compared to feed pre-heating MED, and Rahimi et al. (2014) used multi-stage flash along with MED to increase the distillate production. For all these studies the feed configuration considered was parallel feed. Parallel feed is another variant of parallel/cross feed, where the concentrated brine is discharged from each effect, compared to last effect discharge in parallel/cross feed. Parallel feed is the least energy efficient system compared to parallel/cross or forward feed, as the high temperature brine produced from each effect is directly discharged. For this study we have only considered parallel/cross feed and forward feed.

This paper introduces the novel concept of cogeneration (power and distillate) without negatively affecting sCO_2 Brayton cycle efficiency. The second objective is to identify the optimal feed flow sequence to maximize the distillate production for MED integrated with sensible heat source, and last objective is to study different possibilities for reducing the brine discharge. In addition, an analytical model is formulated for integration of MED with waste heat from sCO_2.

2. System description

Fig. 1 shows a schematic of an sCO_2 recompression cycle. The CO_2 is heated in the heat input section (point 5 and 6), and then enters the turbine (point 6) where it expands and drives the

generator to produce electricity. Low-pressure CO_2 exits the turbine and enters the high-temperature recuperator (point 7) to transfer its heat to the high-pressure stream. After losing heat in the high-temperature recuperator, the sCO_2 enters the low-temperature recuperator (point 8). At the low-temperature recuperator exit, the flow is split between a "recompressor" and the cooler. This recompressor is often included in cycle configurations to improve the effectiveness of the low-temperature recuperator and is explained in more detail by Dostal (2004). The cooler is required to reject heat to the surroundings to complete the closed-loop cycle (point 9) and achieve the design compressor-inlet temperature (point 1). After exiting the compressor at point 1, the high-pressure fluid is heated by the low-temperature recuperator and enters a mixer (point 3) where it combines with the recompressor outlet (point 11) and enters the high-temperature recuperator (point 4). The full high-pressure stream is further heated in the high-temperature recuperator and exits at point 5.

Fig. 2 shows the heat rejection profile for the sCO_2 exiting the low temperature recuperator (grey line). The heat is rejected in range of 80°C and is sufficiently hot to drive a MED system. Fig. 3 shows a schematic of a sCO_2 cycle integrated with MED. The sCO_2 exiting the lo temperature recuperator is cooled in the printed-circuit heat exchanger (PCHE). Because the cross-sectional area of the PCHE channels is very small, an intermediate demineralized water circuit is used to prevent them from clogging (Held et al., 2016). Two PCHEs are used instead of just one to maximize the net heat available for the first effect of the MED (as shown in Fig. 2). The specific heat capacity of the sCO_2 increases with decrease in operating temperature, resulting in higher heat rejection at lower temperature. (In Fig. 2, for a temperature <40°C, the heat rejection is 57% of the entire cycle.) This would result in a very low temperature rise for water, if only one PCHE is used (orange line, Fig. 2). A portion of water coming out of $PCHE_1$ enters $PCHE_2$, resulting in a higher temperature rise. The heated water for $PCHE_2$ enters the MED at temperature $T_{W2,in}$, then leaves the MED at temperature $T_{W2,out}$. It mixes with leftover water stream (W_1-W_2) exiting $PCHE_1$, flows into a plate-and-frame heat exchanger (PFHE), and is cooled by seawater.

In MED, evaporators are placed in series, and the demineralized water stream acts as a heat source for the first effect. For forward feed, the entire feed seawater (F) enters the first MED effect and undergoes partial vaporization in the first effect to produce vapor V_1 and concentrated brine b_1. The vapor V_1 acts as a heat source for the second effect, and the brine

b_1 is the feed for the second effect. This process continues until the last effect. The vapor produced from the last effect flows into the condenser and exits as distillate; similarly, the brine produced in the last effect is discharged from the MED.

3. Process integration for MED

Process integration is often used for optimal energy integration between different system (Klemeš, 2013). Process integration was introduced in the late 1970s to target the energy requirement of the heat-exchanger network (Klemeš and Kravanja, 2013). Using the principle of process integration, one can generate a grand composite curve (GCC), which is a graphical representation of energy integration occurring within the system (Linnhoff and Flower, 1978). GCC is a plot between shifted temperature and the feasible heat transfer occurring between different streams (Bandyopadhyay and Sahu, 2010).

Principle of process integration is also used for energy integration of MED system (Périn-Levasseur et al., 2008; Piacentino and Cardona, 2010). Sharan and Bandyopadhyay (2016b) discussed in detail the methodology for generating the GCC of a MED system and the same principle is used here. Fig. 4 shows the GCC for a 3-effect MED integrated with a demineralized water stream. The demineralized water stream (W_2) acts as a heat source for the MED (line 1-2 in Fig. 4). The net heat available from the demineralized water stream is:

$$\text{Input Energy} = W_2 C_{p,w} T_{W2,in} \tag{1}$$

where $C_{p,w}$ and $T_{w2,in}$ are the specific heat and the temperature of demineralized. Each MED effect is represented by two horizontal lines and a sloped line. The top horizontal line represents the energy required for vapor generation, E_{evap} (shown by line 2-3) and the bottom line represents the condensation, E_{cond} (line 4-5).

$$\mathrm{E}_{evap,n} = \begin{cases} V_1 H_1 + b_1 h_1 - F h_{f,T_1} & n = 1 \\ V_n H_n + b_n h_n - b_{n-1} h_{NEA,n-1} & n \geq 2 \end{cases} \tag{2}$$

$$\text{Vapor Condensation} = V_{n-1} \lambda_{n-1} \tag{3}$$

where V, b, and F are the vapor, brine, and feed flow rate; H and h are vapor and brine enthalpy (Al-Juwayhel et al., 1997); and $h_{f,T1}$ is the feed enthalpy at first effect temperature

T_1. The brine coming from the n-1th effect is at higher pressure; and flashes in the n^{th} effect. While flashing, it faces a slight drop in pressure and temperature, this drop in temperature is called a non-equilibrium allowance (NEA) (Miyatake et al., 1973). $h_{NEA,\, n\text{-}1}$ is the enthalpy of the brine after removing the non-equilibrium allowance. Additional energy integration takes place due to feed pre-heating (line 3-4) and condensate cooling.

$$\text{Feed Pre-heating} = F\left(h_{f,T_1} - h_{f,T_f}\right) \tag{4}$$

$$\text{Condensate Cooling} = V_n C_{p,w}\left(T_{sat,n} - T_{cool}\right) \tag{5}$$

where T_f and T_{cool} are feed and distillate discharge temperature. Once the process stream data for MED and the water stream are calculated, a problem table algorithm (Linnhoff and Flower, 1978) can be used to generate GCC. The point at which GCC touches the y-axis is called the pinch point (points 3, 6, and 7 in Fig. 4 must be touching the y-axis). A pinch point is the bottleneck for the maximum possible energy integration. Sharan and Bandyopadhyay (2016b), proposed that all MED effects must be pinched for minimum energy consumption. However, the paper didn't focus on pinching the background process along with the MED effects.

Fig. 4 shows GCC for two possible cases while integrating MED with a demineralized water stream. For Fig. 4A, the net heat supplied from the water stream is higher (because external cooling of ΔHU is required), whereas for Fig. 4B, external heating is required, apart from the heat coming from the demineralized water. For Fig. 4A, the distillate production can be increased to recover ΔHU, and for Fig. 4B, the distillate production should be decreased to avoid external steam requirement.

To maximize the distillate production without being a parasitic load to the sCO_2 Brayton cycle, the demineralized water stream should be pinched, along with the MED effects. A methodology to pinch the demineralized water stream is developed in the subsequent section.

4. Mathematical formulation for maximum distillate production for forward feed

ACCEPTED MANUSCRIPT

Fig. 5 shows a schematic for the n^{th} effect MED with forward feed. For a feed flow rate of F and the vapor flow rate (V_n) for the n^{th} effect, the brine flow rate (b_n) is given as (Sharan and Bandyopadhyay, 2016c):

$$b_n = F - \sum_{i=1}^{n} V_n \tag{6}$$

Assuming the distillate is salt free, the salt load balance for MED is:

$$b_n X_n = F X_f \tag{7}$$

Using Eq. (6) and Eq. (7), the feed flow rate is:

$$F = V_1 \frac{X_1}{X_1 - X_f} \tag{8}$$

The maximum allowable brine concentration is X_{max}, exiting the last (K^{th}) effect. Using Eq. (7), the brine discharged by the system is:

$$b_K = F \frac{X_f}{X_{max}} \tag{9}$$

Using Eq. (6), Eq. (9) can be written as:

$$\left(F - \sum_{i=1}^{K} V_n \right) X_{max} = F X_f \tag{10}$$

Rearranging Eq. (10) gives:

$$\sum_{i=1}^{K} V_n = \left(\frac{X_{max} - X_f}{X_{max}} \right) F \tag{11}$$

The net distillate (D) produced is:

$$D = \sum_{i=1}^{K} V_n = \left(\frac{X_{max} - X_f}{X_{max}} \right) F \tag{12}$$

The energy balance for the n^{th} effect (from Fig. 5) is given as:

$$V_{n-1} H_{n-1} + b_{n-1} h_{n-1} = V_n H_n + b_n h_n + V_{n-1} h_{cond,n-1}, \quad \forall\ n = 2 \text{ to } n = K \tag{13}$$

ACCEPTED MANUSCRIPT

Using Eq. (6), Eq. (13) can be modified as:

$$V_{n-1}\lambda_{n-1} = V_n H_n + \left(F - \sum_{i=1}^{n} V_n\right) h_n - \left(F - \sum_{i=1}^{n-1} V_{n-1}\right) h_{n-1}, \quad \forall\, n = 2 \text{ to } n = K \tag{14}$$

where λ is the latent heat of evaporation (difference between vapor enthalpy, H_n, and condensate enthalpy, $h_{cond,n}$). Eq. (14) can be further simplified as:

$$V_{n-1}\lambda_{n-1} = V_n (H_n - h_n) + \left(F - \sum_{i=1}^{n-1} V_{n-1}\right)(h_n - h_{n-1}), \quad \forall\, n = 2 \text{ to } n = K \tag{15}$$

The energy required for evaporation in the first effect is:

$$E_{evap,1} = V_1 (H_1 - h_1) - F\left(h_{f,1} - h_1\right) \tag{16}$$

The water stream is shifted away from the pinch point by HU_{water} (see Fig. 4b). Let the first effect of MED be shifted away from the pinch by E_1. The net heat available for integration by the first effect is E_1-HU_{water}. To pinch the first effect and the demineralized water stream, the evaporation occurring in the first effect needs to be changed by a small amount Δ:

$$E_{evap,1} + \left(E_1 - HU_{water}\right) = \left(V_1 + \Delta V_1\right)\left(H_1 - h_1\right) - \left(F_1 + \Delta F_1\right)\left(h_{f,1} - h_1\right) \tag{17}$$

Subtracting Eq. (17) from Eq. (16) gives:

$$\Delta HU = \Delta V_1 \left(H_1 - h_1\right) - \Delta F \left(h_{f,1} - h_1\right) \tag{18}$$

The difference in vapor enthalpy and the feed enthalpy can be approximated as latent heat:

$$\left(H_1 - h_{f,1}\right) \approx \left(H_1 - h_1\right) \approx \lambda_1 \tag{19}$$

Moreover, the feed enthalpy entering the first effect can be approximated as the brine enthalpy leaving the first effect.

$$h_{f,1} \approx h_1 \tag{20}$$

The change in vapor flow rate is:

$$\Delta V_1 \approx \frac{E_1 - HU_{water}}{\lambda_1} \tag{21}$$

ACCEPTED MANUSCRIPT

Using Eq. (8), the change in feed flow rate is:

$$\Delta F \approx \Delta V_1 \left(\frac{X_1}{X_1 - X_f} \right) \tag{22}$$

The change in energy balance for effect 2 is:

$$\Delta V_1 \lambda_1 + (E_2 - E_1) = \Delta V_2 (H_2 - h_2) + \Delta V_1 \left(\frac{X_f}{X_1 - X_f} \right) (h_2 - h_1) \tag{23}$$

Using an approximation like Eq. (19), the change in vapor flow rate for the second effect (ΔV_2) is:

$$\Delta V_2 \approx \frac{(E_2 - HU_{water})}{\lambda_2} \tag{24}$$

Using Eq. (21) and Eq. (24) the change in vapor flow rate for the n^{th} effect can be generalized as:

$$\Delta V_n \approx \frac{(E_n - HU_{water})}{\lambda_n} \tag{25}$$

Using Eq. (11) and Eq. (25),

$$\Delta F = \sum_{i=1}^{K} V_n \left(\frac{X_{max}}{X_{max} - X_f} \right) \tag{26}$$

The new vapor and feed flow rates are:

$$\begin{aligned} V_n^{new} &= V_n + \Delta V_n \\ F^{new} &= F + \Delta F \end{aligned} \tag{27}$$

It can noted that while deriving above equation's it is assumed that $h_{n\text{-}1,\ NEA}$ and $h_{cond,\ n\text{-}1}$ is equivalent to $h_{n\text{-}1}$ using order of magnitude (Sharan and Bandyopadhyay, 2016c), so as to simplify the derivation. However, while generating the process steam data the actual enthalpy values are considered.

ACCEPTED MANUSCRIPT

- Procedure for the integration of MED with the sCO_2 Baryton cycle.

Step 1: Define the input parameters. sCO_2 stream data, MED feed configuration, T_f, minimum effect operating temperature, ΔT_{MED}, ΔT_{PCHE}, X_f, and X_{max}.

Step 2: Mass of water flowing through $PCHE_2$ is calculated on the basis of maximum energy integration with the first effect of the MED.

Step 3: Assume seawater feed flow rate (F) is equal to that of sCO_2 flow rate. Use Eq. (12) to calculate the total distillate generation (D). Assume each effect produces an equal amount of distillate, the initial vapor generation for each effect is:

$$V_n^{initial} = \frac{D}{K} \tag{28}$$

Step 4: Use Eq. (6) and Eq. (7) to calculate the brine flow rate and brine concentration. Generate the GCC. Calculate the amount by which the heated water stream (HU_{water}) and each effect (E_n) is shifted away from pinch.

Step 5: Use Eq. (25) and Eq. (26) to calculate the change in vapor (ΔV_n) and feed flow rate (ΔF_n). Calculate V_n^{new} and F^{new} using Eq. (27).

Step 6: Repeat the procedure from step 5, with new vapor flow rate. The entire procedure is repeated until the solution converges. For convergence, the criterion assumed here is $\Delta V_n < 10^{-5}$ kg/s).

5. Illustrations

The power cycle design parameters are taken from the System Advisory Model developed at National Renewable Energy Laboratory, USA (NREL, 2018), and are listed in Table 1. The power cycle design parameters are listed in Table 1. The sCO_2 cycle parameters are optimized to maximize the system efficiency (Neises and Turchi, 2014) and is 49.2%. sCO_2 exiting the recuperator is at 7.66 MPa, mass flow rate is 979.8 kg/s, and temperature is 79.51°C. 641.8 kg/s of sCO_2 needs to be cooled to 32°C before returning to the compressor and remaining 338 kg/s flows back to the recompressor. The power delivered is 115 MW_e and the net cooling required is 119.1 MW. The input design parameters for MED are listed in Table 2. It may be noted that the thermal losses through MED and sCO_2 power cycle is neglected.

5.1. Heat extraction from sCO_2 power cycle

Fig. 2 shows the net heat available from the sCO_2 stream at different temperatures. As the temperature of sCO_2 decreases, the specific heat capacity increases. For temperatures below 40°C, the net cooling required is about 70 MW. The temperature of the demineralized water in $PCHE_1$ increases from 22°C to 37°C. The heat duty for $PCHE_1$ is 76.1 MW and the water mass flow rate is 1,211 kg/s, with the remaining heat transfer occurring in $PCHE_1$. The temperature of the water flowing through $PCHE_2$ rises from 37°C to 74.6°C. The heat duty for $PCHE_2$ is 43 MW (shown in Fig. 2).

For maximum energy integration between MED and the background process, the effect temperature should be selected in such a way that the energy extraction for each effect is maximum (Sharan and Bandyopadhyay, 2016c). This suggests that each effect should be operated at its minimum possible operating temperature. The first-effect operating temperature (T_1) is 50.3°C, calculated on the basis of the minimum last-effect operating temperature (T_K), temperature driving force for MED (ΔT_{MED}), boiling point rise (BPR) (Al-Juwayhel et al., 1997), and vapor pressure drops (which include pressure drop due to vapor flowing over tube bundles, pressure drop through demister, and pressure drop during condensation). To calculate the different pressure drops, the geometric parameters for MED and correlations are taken from Zhou et al. (2015).

5.2. Integration with forward feed MED

Assuming a feed flow rate equal to that of sCO_2 (i.e., 641.8 kg/s), the net distillate produced (D) is 320.9 kg/s. The vapor generation from each effect is 107 kg/s. The process stream data for the system can be generated and the GCC is drawn. Fig. 6 shows the GCC for the integrated water and MED system. The heated water stream is shifted away from the pinch by 238.5 MW, whereas the effects are shifted away from the pinch by 0.4, 0, and 0.8 MW. Using Eq. (25), the change in vapor flow rate ΔV_1 = -98.7 kg/s, ΔV_2 = -98.38, and ΔV_3 = -97.5 kg/s. The new vapor flow rate is V_1^{new} = 8.2, V_2^{new} = 8.6, and V_3^{new} = 9.5 kg/s. The new feed flow rate for the system is 52.6 kg/s. Once again, the GCC is generated and the procedure is repeated until the solution converges. The GCC for the optimally integrated system is shown in Fig. 7. The demineralized water stream is pinched along with the MED effects. The

temperature of the sCO_2 exiting the MED system is 39.6°C. The network for the integrated system is shown in Fig. 8.

The total distillate generated is 35.3 kg/s (3,045 m^3/day). The net pumping required for 3-effect MED is 2.41 kWh/m^3. The pumping power is calculated using various pressure-head (preheater, brine, distillate, condensate, and chemical dosing) correlations from Christ et al. (2015). The distillate produced from the first effect is 10.2 kg/s. The evaporation from the second effect occurs in two parallel effects (2A and 2B). The vapor produced in the first effect loses its latent heat in the second effect 2A; for effect 2B, the heat source is the demineralized water stream exiting preheater 1, which is a sensible heat source. Evaporators 2A and 2B produce 10.37 kg/s and 1.36 kg/s distillate. The specific evaporator area to produce a unit amount of distillate in 2A is 357 m^2/kg/s and for 2B is 510 m^2/kg/s (because of the low heat-transfer coefficient for evaporator 2B). Similarly, the third effect is divided into effects 3A and 3B. Distillate generated by them is 11.8 kg/s and 1.45 kg/s and the required evaporator specific area is 370 m^2/kg/s and 525 m^2/kg/s. Evaporators 2B and 3B are not producing a sufficient amount of distillate compared to their area requirement, and the sensible-heating evaporators 2B and 3B complicate the system. Hence, evaporators 2B and 3B are removed from the network, as shown in Fig. 9.

The final design parameters are listed in Table 3. The modified network is quite simple compared to the fully integrated system, and the number of feed preheaters is reduced from four to one (Fig. 9). A comparison between the two configurations (Fig. 8 and Fig. 9) is shown in Table 3. Removing the sensible heating evaporators 2B and 3B reduces the distillate production by 12%. With reduced distillate production and the removal of the sensible-heating evaporator, the evaporator heating area requirement is reduced by 16.6% and the condenser area by 20.1%. Moreover, the MED systems are commercially manufactured based on equal evaporator area; with intermediate sensible-heating evaporators the evaporator area progressively increases from the first to the last effect. It will be difficult to commercially manufacture such a MED system.

5.3. Parallel/cross feed MED

In parallel/cross feed MED, the feed with almost equal flow rate enters into each MED effect. Table 4 shows the difference between the parallel/cross feed and forward-feed MED systems for the simplified network (without intermediate sensible heating evaporators). For parallel/cross feed, each MED effect is operating at the maximum brine concentration, leading to a high boiling point rise for each effect (Al-Juwayhel et al., 1997); this results in a higher effect operating temperature. For a 3-effect parallel/cross feed, the first-effect operating temperature is 50.9°C, compared to 50.3°C for forward feed. Higher first-effect operating temperature reduces the energy integration with the sCO_2 power cycle. Additionally, the feed pre-heating for forward feed is 8.28 MW, compared to 7.14 MW for parallel/cross feed. This is because for forward feed, the entire feed gets pre-heated to the first-effect operating temperature. On the other hand, for parallel/cross feed, about F/K of the feed is pre-heated to the first-effect operating temperature, where K is the number of MED effects (3-effect for present case. The net heat transferred from the demineralized to MED is 32.6 MW and 30.78 MW for forward feed and parallel/cross feed. Higher heat transfer increases the distillate produced by 3.9% for forward feed.

Often, the efficiency of MED is measured in terms of gain output ratio (*GOR*) and is defined the ratio of net distillate produced to external steam supplied. To measure the *GOR* with a sensible heat source a term $GOR_{sensible}$ is introduced, and is defined as:

$$GOR_{sensible} = \frac{D}{M_{s,sensible}} = \frac{D}{\left(\frac{W_2 C_{pw} \left(T_{W2,in} - T_{W2,out} \right)}{\lambda_1} \right)} \tag{29}$$

where $M_{s,sensible}$ is the equivalent amount of steam supplied to the MED, and is the ratio of net heat supplied by demineralized steam to MED to the latent heat of the first effect . For MED with steam as an external heat source, parallel/cross feed has a higher GOR compared to forward feed (Sharan and Bandyopadhyay, 2016b) and the same trend can be observed with $GOR_{sensible}$ as well, 1.8% higher for parallel/cross feed. For MED with given amount of steam, parallel/cross feed will produce more distillate than forward feed.

The specific evaporator and condenser area requirement for MED is slightly higher for parallel/cross feed compared to forward feed. The number of feed preheaters required for

parallel/cross feed MED is three, compared to only one feed preheater for forward feed, which results in reducing the pumping power by 1%. It is safe to conclude that the sCO_2 Brayton cycle should always be integrated with forward-feed MED compared to parallel/cross feed when intermediate sensible-heating evaporators are not present. In other words, for MED integrated with a sensible heating source cooled to a temperature lower than the first-effect operating temperature, forward feed yields higher distillate production.

5.4. Variation in number of MED effects

Fig. 10a shows the results for variation in first effect operating temperature with number of operating MED effects for forward and parallel/cross feed. With increase in number of operating effects, the effect operating temperature increases. For forward feed the first effect operating temperatures for 2 and 7-effect MED is 46.6°C and 64.9°C (shown in Fig. 10a). As already discussed the parallel/cross feed have higher brine concentration and they operate at slightly higher temperature compared to forward feed. For 2 and 7-effect MED the first effect temperature for parallel/cross feed is 46.9°C and 66.4°C.

Fig 10b and 10c shows comparison between feed pre-heating and the net heat transferred for forward feed and parallel/cross feed with number of MED effects. Feed pre-heating for forward feed is 7.5% higher for 2-effect and 52.6% higher for 7-effect MED. For forward feed the feed pre-heating is a function of feed flowrate and first effect operating temperature. Maximum feed pre-heating for forward feed is for 5-effect MED (11.5 MW).

The net heat transferred is the summation of feed pre-heating and energy available for the first MED effect. The net energy available for the first effect is inversely proportional to the first effect operating temperature. The net energy available for the first effect also dictates the net feed flowrate which in turn influences the feed pre-heating. So, the net heat transferred is strongly dependent on the first effect operating temperature, and as the number of effects increases the net heat transferred decreases. For forward feed due to lower effect operating temperature and higher feed pre-heating, the net heat transferred is higher compared to parallel/cross feed.

The net distillate produced is a function of net heat transferred and number of operating effects. For a constant heat supplied, distillate production is directly proportional to number

of operating effects. For present study the net heat supplied decreases with increase in number of effects, and the maximum distillate production occurs at 4-effect MED for both feed configuration. For forward feed the maximum distillate production is 3041 m^3/d and is 7.5% higher compared to parallel/cross feed (as shown in Fig 10d).

The $GOR_{sensible}$ for parallel/cross feed is higher than forward feed (as shown in Fig. 10e). For 7-effect parallel/cross feed the $GOR_{sensible}$ is 6.87, whereas for forward feed is 3.5. This is due to the fact the substantial portion of sensible heat is goes in feed pre-heating for forward feed. For a fully integrated system parallel/cross feed MED would be more energy efficient compared to forward feed,

Fig. 10F shows the cost comparison between forward feed and parallel/cross feed with variation in MED effect. The capital and operating cost for MED is calculated using Desaldata (2018), heat exchanger and pump cost from (Esfahani et al., 2014). The electricity price is assumed to be 10.5 cents/kWhr and annual discount rate of 8%. The minimum distillate cost for forward feed is 1.06 \$/m^3 (4-effect) and for parallel feed is 1.09 \$/m^3 (4-effect).

Based on the result presented in Fig 10, 4-effect forward feed is the optimal MED producing 7.5% higher distillate production at 2.6% cheaper cost.

6. Reduction in brine discharge

For seawater desalination, the brine produced from MED is generally discharged directly into the sea. Pre-treatment chemicals, high salinity, heavy metal, and temperature of the brine rejected from the desalination system often lead to critical environmental issues (Giwa et al., 2017). The other solution can be brine disposal, which is expensive, with costs ranging from 5% to 33% of the total desalination cost (Ahmed et al., 2001a). Naseri et al. (2017) used electrolyzer for concentrating the brine coming out from the reverse osmosis system. Increasing the brine outlet concentration leads to reduced brine flow rate, resulting in lower pumping cost, reduced brine disposal cost and can also help in achieving zero liquid discharge. Onishi et al. (2017) developed a model for MED integrated with heat pumps for achieving zero liquid discharge. With thermal heat source, the brine concentration can be

increased by increasing the maximum allowable brine concentration or by recycling the brine produced from the last effect. A comparison between operating MED at maximum brine concentration and brine recycling is done in this section.

6.1 Maximum brine concentration

Decreasing the brine concentration decreases the distillate recovery ratio, which is the maximum amount of freshwater that can be extracted from seawater to the amount of water present in the discharged brine, and it is given as:

$$\text{Recovery Ratio} = 1 - \frac{X_f}{X_{max}} \left(\frac{1 - \frac{X_{max}}{10^6}}{1 - \frac{X_f}{10^6}} \right) \tag{30}$$

For the base case of 70,000 ppm, the recovery ratio is 51.8%. The maximum brine salinity is a function of effect operating temperature (EL-Dessouky et al., 2000) and is given as:

$$X_{max} = 0.9\left(457628.5 - 11304.11T_K + 107.5781T_K^2 - 0.360747T_K^3\right) \tag{31}$$

For a last-effect temperature (T_K) of 42.8°C, the maximum brine concentration is 142,600 ppm. Fig. 11 shows the variation in MED performance with maximum brine concentration, with the variations shown with respect to the base case of 70,000 ppm. With an increase in brine concentration, the recovery ratio increases, leading to a reduced feed seawater requirement. At 50,000 ppm, the feed flow rate required is 70% higher, whereas at 142,600 ppm, the feed flow rate is reduced by 35.2%. Reducing the feed flow rate reduces the pumping power requirement for the MED; at 142,600 ppm, the pumping power is only 1.96 kWh/m^3, which is 9% lower than the base and 17.8% higher at 50,000 ppm. Increasing the brine concentration increases the *BPR* for each effect, leading to reduced energy integration with the sCO_2 power cycle. This result to a slight reduction in distillate production by 2.1% at 140,000 ppm and an increase in distillate production by 2.1% at 50,000 ppm. The evaporator area requirement is almost constant with brine concentration. Higher brine concentration helps to reduce the net brine discharge, which is very useful in achieving zero liquid discharge. For 140,000 ppm, the brine discharge is 68.2% lower than that at 70,000 ppm.

Instead of discharging the brine directly into the sea, which could cause critical environmental issues, the brine can be sent directly to the evaporation pond to achieve zero liquid discharge. The evaporation pond is used to naturally evaporate the water present in the discharged brine. An evaporation pond is ideally suited for a region with high solar radiation, cheap land availability, and terrain quality (Morillo et al., 2014). For an evaporation pond having a net evaporation rate of 2 gpm per acre (0.00187 lpm/m^2) (Mickley, 2009), the net pond area required is 925,347 m^2 for treating the 31 kg/s of brine at 70,000 ppm. Increasing the brine concentration can significantly reduce the evaporation pond size: at 142,600 ppm, the pond size reduces to 241,548 m^2 (70.4% reduction, as shown in Fig. 10).

The major demerit of higher brine concentration is the increased maintenance cost. Moreover, beyond 120,000 ppm, there is a slight improvement in system performance. All these factors suggest that forward-feed MED should be operated in the range of 120,000 ppm to reduce the amount of seawater intake, brine discharge, and environmental impacts, and to achieve zero liquid discharge.

6.2 Brine recycling

To reduce the brine discharge from MED, a portion of brine exiting the last effect can be recycled and mixed with the incoming feed. This leads to a reduced brine flow rate and feed flow rate, and an increased feed water temperature entering the MED system. Fig. 12 shows the variation in system performance with variation in brine recycling ratio (*R*). The brine recycling ratio is given as:

$$\mathrm{R} = \frac{\text{Brine recycled}}{\text{Brine coming out from last effect}} \tag{32}$$

A detailed derivation for brine recycling is given in Appendix A1. With an increase in brine recycling, the outlet concentration for MED is increased. The ratio of feed concentration entering the first effect to the discharged brine concentration is kept constant at 0.5. The maximum recycling allowed is limited by the maximum allowable brine concentration. At 142,600 ppm, the maximum brine recycling is 0.675. The variation in MED performance shown in Fig. 11 is represented in terms of the ratio with respect to the base case of $R = 0$.

With an increase in *R*, the feed flow rate decreases. And with a reduction by 54% at *R* = 0.675, the pumping power for MED reduces by 10.5%. The net brine discharged also decreases with an increase in *R* and is reduced by 69.5% at maximum brine recycling. An increase in recycling ratio increases the feed concentration, increases *BPR*, reduces energy integration, and eventually reduces distillate production. The distillate production is reduced by 6.3% at *R* = 0.675. The specific evaporator area remains almost constant with *R*. With an increase in recycling, the feed and brine flow rates decreases substantially, but the distillate production also decreases simultaneously.

Table 5 shows the comparison between no brine recycling and brine recycling with the same maximum brine concentration. For 80,000 ppm brine concentration, the maximum recycling allowed is 0.22, whereas for 120,00 ppm, maximum recycling is 0.67. With an increase in brine recycling, the amount of feed flow rate decreases: at 120,000 ppm, the feed flow rate decreases by 19.4%, but the pumping power is reduced by only 0.7% because a substantial amount of brine must be recycled. With an increase in brine recycling, the feed concentration increases, leading to an increase in *BPR* and reduced distillate production by 2.5%. Moreover, to recycle the brine, additional pumps and pipe are needed. The only benefit observed for brine recycling is reduction in feed flow rate, with almost no saving in pumping power for seawater desalination. Brine recycling may be useful for brackish-water desalination, where the pumping power required for feed water is quite significant.

7. Conclusion

The sCO_2 Brayton cycle has the potential to generate electricity more efficiently than conventional steam-Rankine cycles. The cycle also benefits from sensible heat rejection that is sufficient to drive a thermal desalination system. This paper introduces the concept of integrating a multi-effect distillation system with a sCO_2 power cycle. The distillate is generated without being a parasitic load to the power cycle (without loss in energy efficiency).

Generally, with steam as a heating source, the parallel/cross feed is the most energy-efficient feed flow sequence for MED. However, the current study shows that with a sensible heat

source (sCO_2) forward feed yields a more energy-efficient solution. This is due to the lower effect operating temperature and higher feed preheating for the forward-feed configuration. For the case study considered, 4-effect MED gives maximum distillate production of 3041m^3/d at 1.06 \$/m^3, at a constant power plant efficiency of 49.2%. The distillate produced by forward feed is 7.5% higher and 2.6% cheaper compared to parallel/cross feed configuration.

For reducing the brine flowrate two possible methods are considered brine recycling and increasing the maximum brine concentration. For seawater desalination, increasing the maximum brine concentration is more beneficial because it yields more distillate with almost the same pumping power required as in brine recycling.

The principle of process integration is used for cogeneration. An analytical methodology to maximize the distillate production without being a parasitic load for the power plant is derived. Although the paper focuses on integration of MED with sCO_2 Brayton cycle, the same methodology can be applied for integration of MED with any sensible heat source. Future research work is directed toward development of model to predict the annual performance of the system and integration with solar thermal powered sCO_2 Brayton cycle.

Acknowledgement

The research work was supported by the internal funding (Laboratory Directed Research and Development Program) at National Renewable Energy Laboratory.

ACCEPTED MANUSCRIPT

ACCEPTED MANUSCRIPT

Appendix: Model with brine recycling

Let the brine recycling ratio be *r* and is defined as the ratio of mass flowrate of brine recycled to net brine produced. Mass of brine recycled (F_r) is

$$F_r = rb_K \tag{A1}$$

where, b_K is the mass of brine generated from the last effect. The mass balance for the mixer is given as:

$$F_{in} = F + F_r \tag{A2}$$

where, F_{in} is the feed flow rate of seawater mixed with brine and F is the seawater feed flow rate. The salt load balance for the mixer is:

$$FX_F + F_r X_K = F_{in} X_{in} \tag{A3}$$

where, X_{in} is the brine concentration after mixing. b_K can be calculated using Eq. (9) and is:

$$b_K = \sum_{i=1}^{K} F_i \frac{X_{in}}{X_K} = F_{in} \frac{X_{in}}{X_K} \tag{A4}$$

Solving Eq's. (A1-A4), X_{in} is:

$$X_{in} = \frac{X_f X_K}{X_K - r\left(X_K - X_f\right)} \tag{A5}$$

Similarly, the mass of feed seawater supplied is:

$$F = F_{in} \frac{1}{1 + \left(1 - r\right)\frac{X_f}{X_K}} \tag{A6}$$

Temperature of mixed seawater (T_{in}) is:

$$T_{in} = T_f + \left(T_K - T_f\right)\left(\frac{rX_K}{X_K - r\left(X_K - X_f\right)}\right) \tag{A7}$$

References

Ahn, Y., Bae, S.J., Kim, M., Cho, S.K., Baik, S., Lee, J.I., Cha, J.E., 2015. Review of supercritical CO2 power cycle technology and the current status of research and development. Nucl. Eng. Technol. 47, 647–661.

Al-Juwayhel, F., El-Dessouky, H., Ettouney, H., 1997. Analysis of single-effect evaporator desalination systems combined with vapor compression heat pumps. Desalination 114, 253–275.

Bandyopadhyay, S., Sahu, G.C., 2010. Modified problem table algorithm for energy targeting. Ind. Eng. Chem. Res. 49, 11557–11563.

Bauer, M.L., Vijaykumar, R., Lausten, M., Stekli, J., 2016. Pathways to cost competitive concentrated solar power incorporating supercritical carbon dioxide power cycles, in: The 5th International Supercritical CO2 Power Cycles Symposium. San Antonio, pp. 1–22.

Brun, K., Friedman, P., Dennis, R., 2017. Fundamentals and Applications of Supercritical Carbon Dioxide (sCO2) Based Power Cycles. Woodhead Publishing/Elsevier, Cambridge, USA.

Christ, A., Regenauer-lieb, K., Tong, H., 2015. Boosted Multi-Effect Distillation for sensible low-grade heat sources : A comparison with feed pre-heating Multi-Effect Distillation. Desalination 366, 32–46.

Conboy, T., Fuller, R., 2012. Performance characteristics of an operating supercritical CO2 Brayton cycle. J. Eng. gas turbines power 134, 1–12.

DOE, 2016. Department of Energy, USA. URL energy.gov/under-secretary-science-and-energy/articles/doe-announces-80-million-investment-build-supercritical (accessed 4.18.18).

Dostal, V., 2004. A Supercritical Carbon Dioxide Cycle for Next Generation Nuclear Reactors. Massachusetts Institute of Technology, Cambridge, USA.

EL-Dessouky, H.T., Ettouney, H.M., Yhel, F.A.L.J., 2000. Multiple effect evaporation-vapour compression desalination processes. IChem 78, 662–676.

Engineering page. URL www.engineeringpage.com/technology/thermal/transfer.html

(accessed 4.18.2018).

Esfahani, I.J., Kang, Y.T., Yoo, C., 2014. A high efficient combined multi-effect evaporation- absorption heat pump and vapor-compression refrigeration part 1 : Energy and economic modeling and analysis. Energy 75, 312–326.

Held, T.J., Miller, J., Buckmaster, D.J., 2016. A comparative study of heat rejection systems for sCO2 power cycles, in: The 5th International Symposium - Supercritical CO2 Power Cycles. Texas.

Hinze, J.F., Nellis, G.F., Anderson, M.H., 2017. Cost comparison of printed circuit heat exchanger to low cost periodic flow regenerator for use as recuperator in a s-CO2 Brayton cycle. Appl. Energy 208, 1150–1161.

IDA. Desaldata. URL www.desaldata.com/cost_estimator (accessed 4.18.2018).

Ihm, S., Al-Najdi, O.Y., Hamed, O.A., Jun, G., Chung, H., 2016. Energy cost comparison between MSF, MED and SWRO: Case studies for dual purpose plants. Desalination 397, 116–125.

Jaroslav, H., Lilian, K., Christian, O., 2011. Thermoelectric energy storage based on transcritical CO2 cycle, in: Supercritical CO2 Power Cycle Symposium. Boulder, Colorado, pp. 2–6.

Klemeš, J.J., 2013. Handbook of process integration (PI): minimisation of energy and water use, waste and emissions. Woodhead Publishing/Elsevier, Cambridge, UK.

Klemeš, J.J., Kravanja, Z., 2013. Forty years of heat integration: Pinch analysis (PA) and mathematical programming (MP). Curr. Opin. Chem. Eng. 2, 461–474.

Kouta, A., Al-sulaiman, F.A., Atif, M., 2017. Energy analysis of a solar driven cogeneration system using supercritical CO2 power cycle and MEE-TVC desalination system. Energy 119.

Lee, W.W., Bae, S.J., Jung, Y.H., Yoon, H.J., Jeong, Y.H., Lee, J.I., 2017. Improving power and desalination capabilities of a large nuclear power plant with supercritical CO2 power technology. Desalination 409, 136–145.

Lehar, M.A., Michelassi, V., 2013. System and method for recovery of waste heat from dual heat sources. US 2013/0247570 A1.

Linnhoff, B.O.D., Flower, J.R., 1978. Synthesis of Heat Exchanger Networks. AIChE 24, 633–642.

Mickley, M.C., 2009. Treatment of Concentrate, U.S. Department of the Interior Bureau of Reclamation. Denver, USA.

Miyatake, O., Murakami, K., Kawata, Y., Fujii, T., 1973. Fundamental experiments with flash evaporation. Heat Transf. Res 2, 89–100.

Naseri, A., Bidi, M., Ahmadi, M.H., 2017. Exergy analysis of a hydrogen and water production process by a solar-driven transcritical CO2 power cycle with Stirling engine. J. Clean. Prod. 113, 1215–1228.

National Renewable Energy Laboratory (NREL). System advisor model version 2016.3.14. URL sam.nrel.gov/content/downloads (accessed 4.18.2018).

Neises, T., Turchi, C., 2014. A comparison of supercritical carbon dioxide power cycle configurations with an emphasis on CSP applications. Energy Procedia 49, 1187–1196.

Onishi, V.C., Ruiz-Femenia, R., Salcedo-Díaz, R., Carrero-Parreño, A., Reyes-Labarta, J.A., Fraga, E.S., Caballero, J.A., 2017. Process optimization for zero-liquid discharge desalination of shale gas flowback water under uncertainty. J. Clean. Prod. 164, 1219–1238.

Ortega-Delgado, B., García-Rodríguez, L., Alarcón-Padilla, D.C., 2016. Thermoeconomic comparison of integrating seawater desalination processes in a concentrating solar power plant of 5 MWe. Desalination 392, 102–117.

Périn-Levasseur, Z., Palese, V., Maréchal, F., 2008. Energy integration study of a multi-effect evaporator, in: Proceedings of the 11th Conference on Process Integration Modelling and Optimisation for Energy Saving and Pollution Reduction. pp. 1–17.

Piacentino, A., Cardona, E., 2010. Advanced energetics of a Multiple-Effects-Evaporation (MEE) desalination plant. Part II: Potential of the cost formation process and prospects for energy saving by process integration. Desalination 259, 44–52.

Rahimi, B., Christ, A., Regenauer-lieb, K., Tong, H., 2014. A novel process for low grade heat driven desalination. Desalination 351, 202–212.

Sabau, A.S., Yin, H., Qualls, L.A., Mcfarlane, J., 2011. Investigations of supercritical CO2

Rankine cycles for geothermal power plants, in: Supercritical CO2 Power Cycle Symposium. Boulder, pp. 1–8.

Sharan, P., Bandyopadhyay, S., 2017. Energy integration of multiple-effect evaporator, thermo-vapor compressor, and background process. J. Clean. Prod. 164, 1192–1204.

Sharan, P., Bandyopadhyay, S., 2016a. Solar assisted multiple-effect evaporator. J. Clean. Prod. 142, 2340–2351.

Sharan, P., Bandyopadhyay, S., 2016b. Energy optimization in parallel/cross feed multiple-effect evaporator based desalination system. Energy 111, 756–767.

Sharan, P., Bandyopadhyay, S., 2016c. Integration of multiple effect evaporators with background process and appropriate temperature selection. Ind. Eng. Chem. Res. 55, 1630–1641.

Tse, L.A., Neises, T., 2016. Analysis and optimization for off-design performance of the recompression sCO2 cycles forhigh temperature CSP applications, in: The 5th International Symposium-Supercritical CO2 Power Cycles. San Antonio, pp. 1–13.

Wang, Y., Lior, N., 2011. Thermoeconomic analysis of a low-temperature multi-effect thermal desalination system coupled with an absorption heat pump. Energy 36, 3878–3887.

Zhou, S., Guo, Y., Mu, X., Shen, S., 2015. Effect of design parameters on thermodynamic losses of the heat transfer process in LT-MEE desalination plant. Desalination 375, 40–47.

ACCEPTED MANUSCRIPT

ACCEPTED MANUSCRIPT

List of Table captions

Table 1. Design parameters for the power cycle (NREL, 2018)

Table 2: Design parameters for MED

Table 3: Comparison between MED with and without sensible-heating evaporators

Table 4: Comparison between forward-feed and parallel/cross feed MED with 3-effect

Table 5: Comparison between no brine recycling and brine recycling

ACCEPTED MANUSCRIPT

ACCEPTED MANUSCRIPT

Table 1. Design parameters for the power cycle (NREL, 2018)

Input parameters		**Optimized design parameters**	
Net power output	115 MW_e	Compressor outlet pressure	25 MPa
Turbine inlet temperature	600°C	Compressor inlet pressure	7.66 MPa
Maximum pressure	25 MPa	Recompression fraction	0.345
Turbine isentropic efficiency	0.915	Conductance allocated to low-temperature recuperator	13.8 MW_t/K
Main compressor inlet temperature	32°C	**Calculated cycle metrics**	
Compressor isentropic efficiency	0.85	Cycle efficiency	49.2%
Total recuperator conductance	23 MW_t/K	sCO_2 mass flowrate through cooler	641.8 kg/s

Table 2: Design parameters for MED

sCO_2 inlet pressure	7.66 MPa
sCO_2 mass flow rate	641.8 kg/s
sCO_2 inlet temperature	79.51^oC
sCO_2 exit temperature	32^oC
Feed temperature	17^oC
Feed concentration	35,000 ppm
Brine concentration	70,000 ppm
Last-effect temperature (Sharan and Bandyopadhyay, 2017)	42.8^oC
Minimum-temperature driving force for MED heat exchangers (ΔT_{MED}) (Sharan and Bandyopadhyay, 2016a)	3^oC
Minimum-temperature driving force for PCHE (ΔT_{PCHE}) (Held et al., 2016)	3^oC
Heat-transfer coefficient for sensible-heating evaporator (Engineeringpage, 2018)	1 kW/m^2K

Table 3: Comparison between MED with and without sensible-heating evaporators

	Evaporator 2B and 3B present	Evaporator 2B and 3B removed	Difference (%)
Distillate (m^3/d)	35.3	31.02	-12
Cooling required (MW)	78.8	86.5	9.7
Evaporator area (m^2)	11,929	9,950	-16.6
Condenser area (m^2)	985	788	-20.1
Pre-heater area (m^2)	1557	901	-42.1
Brine cooler area (m^2)	208	183	-11.6
PFHE area (m^2)	13215	13468	1.92
Number of preheater	4	1	-75

Table 4: Comparison between forward-feed and parallel/cross feed MED with 3-effect

	Forward Feed	Parallel/Cross Feed	% change
Distillate [kg/s]	31.02	29.83	3.86
Net heat transferred (MW)	32.6	30.78	5.6
$M_{s,senible}$(kg/s)	13.68	12.91	5.59
$GOR_{sensible}$	2.27	2.31	-1.84
Evaporator specific area (m^2/kg/s)	320.7	323.7	-0.93
Condenser specific area (m^2/kg/s)	25.5	25.7	-0.59
HE specific area including PFHE (m^2/kg/s)	469	488.9	-4.22
Specific pumping power (kWh/m^3)	2.28	2.31	-1.4
First-effect temperature (°C)	50.3	50.9	-1.16
First-effect brine concentration (ppm)	41,895	70,000	40.1
Second-effect brine concentration (ppm)	52,356	70,000	25.2
Third-effect brine concentration (ppm)	70,000	70,000	0

ACCEPTED MANUSCRIPT

ACCEPTED MANUSCRIPT

Table 5: Comparison between no brine recycling and brine recycling

	No recycling	With recycling	% change	No recycling	With recycling	% change	No recycling	With recycling	% change	No recycling	With recycling	% change
X_{max} (ppm)	80,000	80,000		100,000	100,000		120,000	120,000		142,600	142,600	
R	0.00	0.22		0.00	0.46		0.00	0.59		0.00	0.67	
Feed (kg/s)	54.9	53.9	-1.8%	47.1	42.4	-10.1%	43.0	34.7	-19.4%	40.2	28.5	-29.1%
Distillate (kg/s)	30.9	30.8	-0.3%	30.6	30.3	-1.2%	30.5	29.7	-2.5%	30.4	29.1	-4.2%
A_{evap} (m^2/kg/s)	321.3	321.0	-0.1%	322.0	321.5	-0.2%	322.4	322.1	-0.1%	322.7	322.8	0.0%
Pump (kW)	2.1	2.1	0.0%	2.0	2.0	-0.4%	2.0	2.0	-0.7%	2.0	1.9	-0.7%
Brine flowrate (kg/s)	24.0	23.9	-0.3%	16.5	16.3	-1.2%	12.6	12.2	-2.5%	9.9	9.5	-4.2%

ACCEPTED MANUSCRIPT

List of Figure captions

Fig. 1: Schematic for a once-through cooled sCO_2 recompression Brayton cycle.

Fig. 2: Heat transfer between sCO_2 and water streams.

Fig. 3: Schematic for MED integrated with sCO_2 Brayton cycle.

Fig. 4: GCC for MED integrated with sCO_2 indirectly via demineralized water loop. (a) Demineralized water stream requires external cooling because of insufficient flow of thermal desalination. (b) External utility is required because of excessive distillate production.

Fig. 5: Schematic for the n^{th}-effect MED.

Fig. 6: GCC for MED integrated with sCO_2 stream with feed flow rate equal to sCO_2 flow rate.

Fig. 7: GCC for MED optimally integrated with sCO_2 stream

Fig. 8: Network for MED integrated with heated water, with sensible-heating evaporators 2B and 3B.

Fig. 9: Network for MED integrated with heated water, without sensible-heating evaporators 2B and 3B.

Fig. 10: Results for variation in number of MED effects on (a) the first effect operating (b) Feed pre-heating (c) net heat transferred (d) Gain output ratio (e) net distillate produced, and (f) distillate cost for forward and parallel/cross feed.

Fig. 11: Variation in MED performance with maximum brine concentration.

Fig. 12: Variation in MED performance with brine recycling.

ACCEPTED MANUSCRIPT

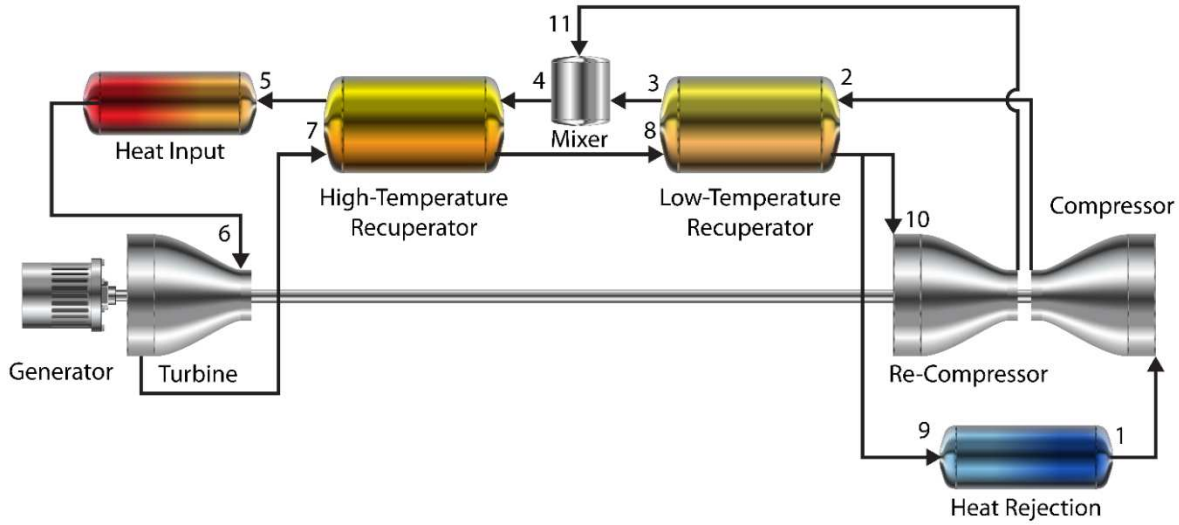

Fig. 1: Schematic for a once-through cooled sCO_2 recompression Brayton cycle.

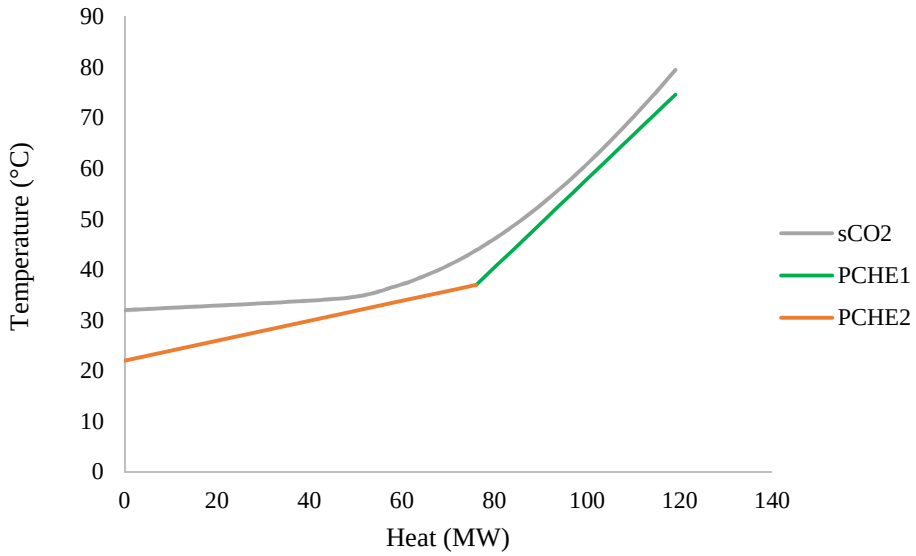

Fig. 2: Heat transfer between sCO_2 and water streams.

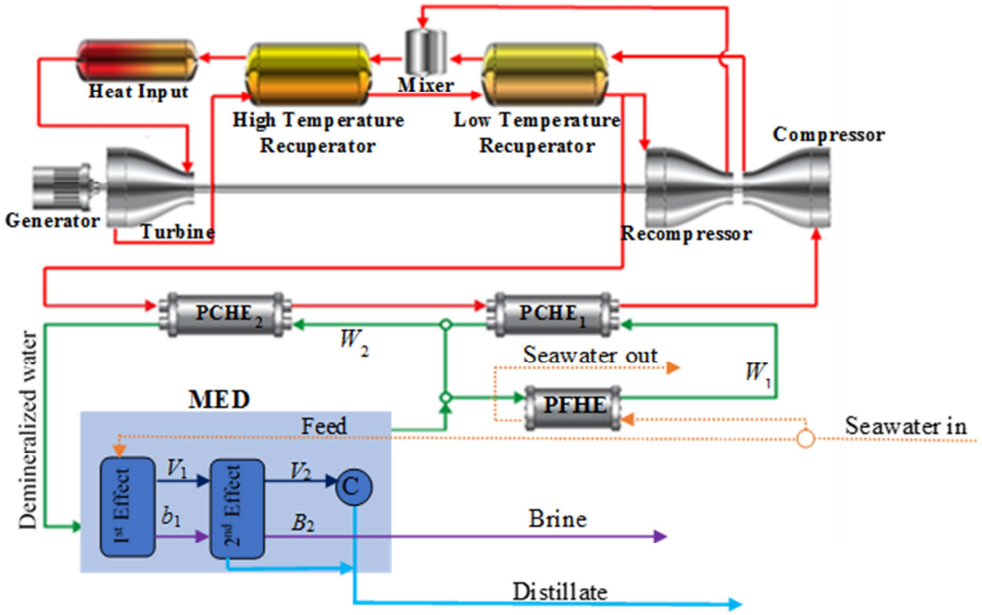

Fig. 3: Schematic for MED integrated with sCO_2 Brayton cycle.

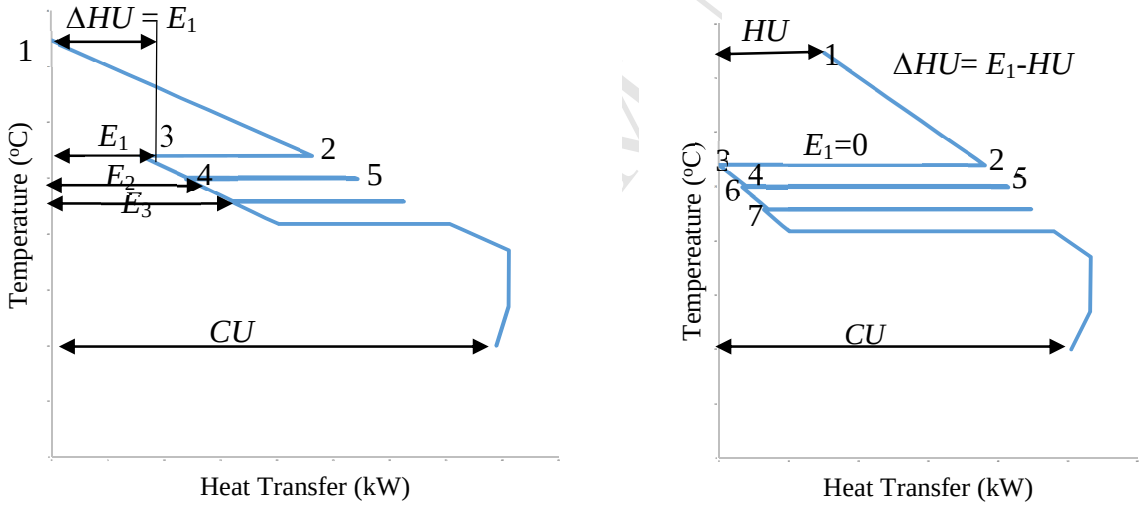

(a) (b)

Fig. 4: GCC for MED integrated with sCO_2 indirectly via demineralized water loop. (a) Demineralized water stream requires external cooling because of insufficient flow of thermal desalination. (b) External utility is required because of excessive distillate production.

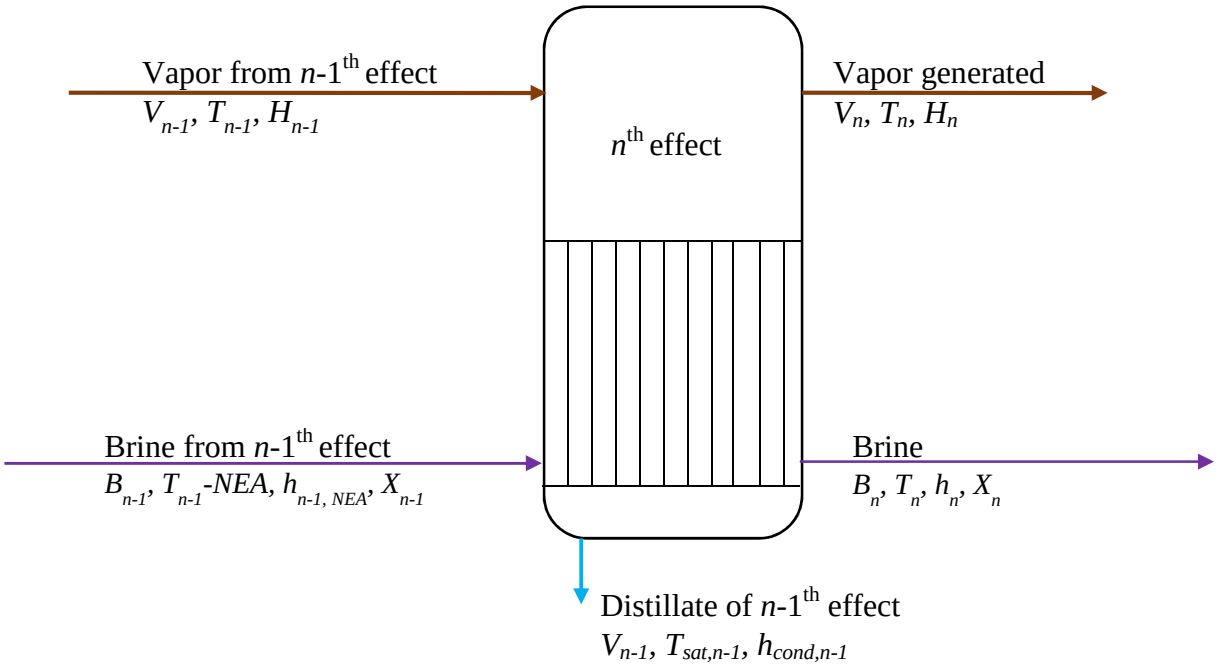

Fig. 5: Schematic for the nth-effect MED.

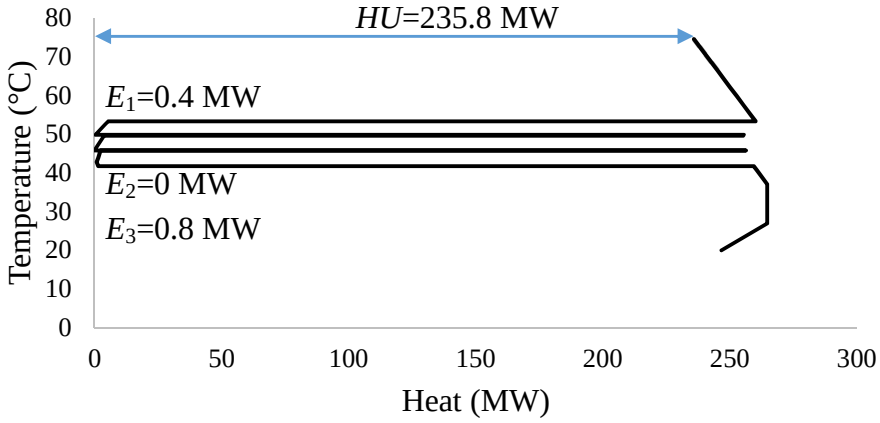

Fig. 6: GCC for MED integrated with sCO_2 stream with feed flow rate equal to sCO_2 flow rate.

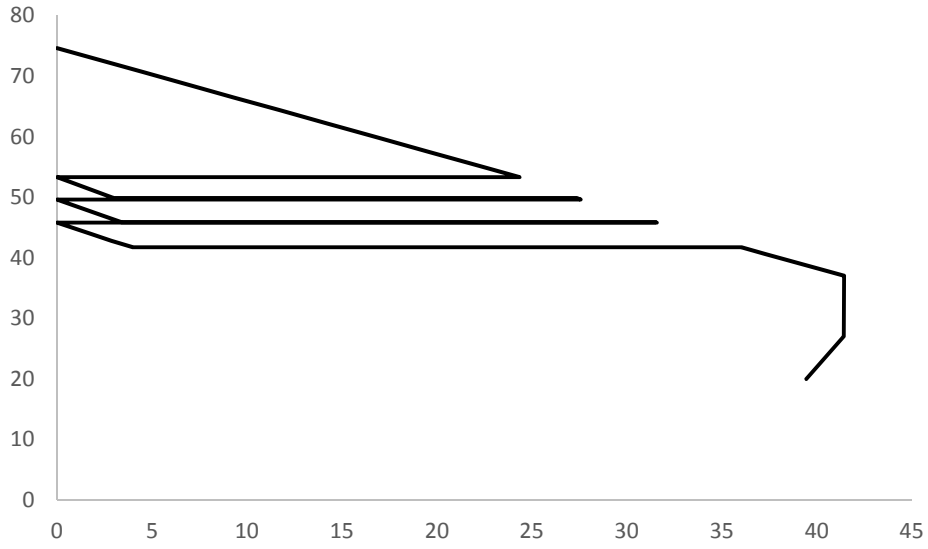

Fig. 7: GCC for MED optimally integrated with sCO_2 stream

ACCEPTED MANUSCRIPT

ACCEPTED MANUSCRIPT

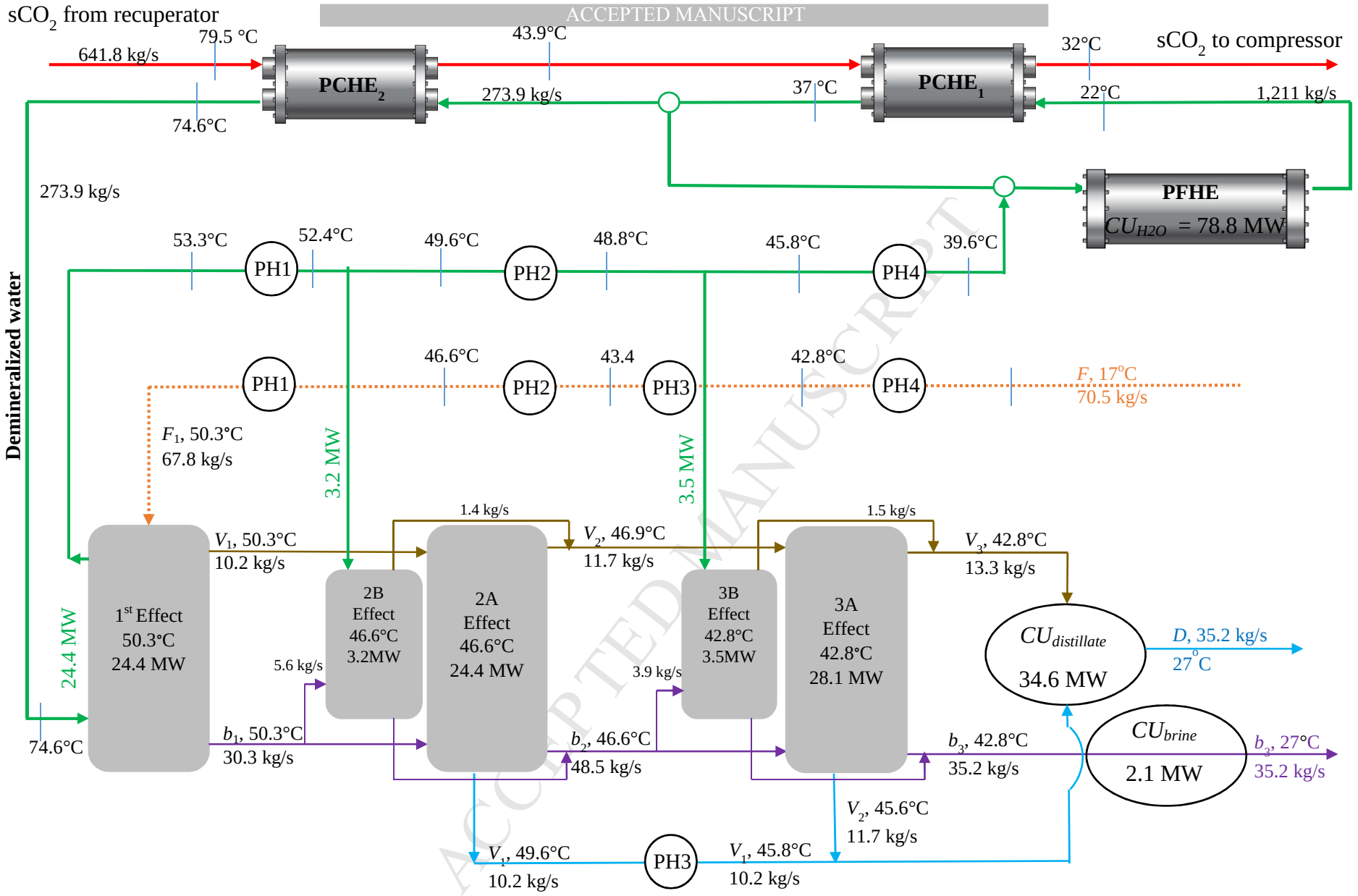

Preheater Duty

PH1= 1.04 MW	PH2= 0.91 MW
PH3 = 0.17 MW	PH4 = 7.3 MW

Symbol

37

Hot stream — Demineralized water

Feed — Vapor

Brine — Vapor Condensate

Fig. 8: Network for MED integrated with heated water, with sensible-heating evaporators 2B and 3B.

ACCEPTED MANUSCRIPT

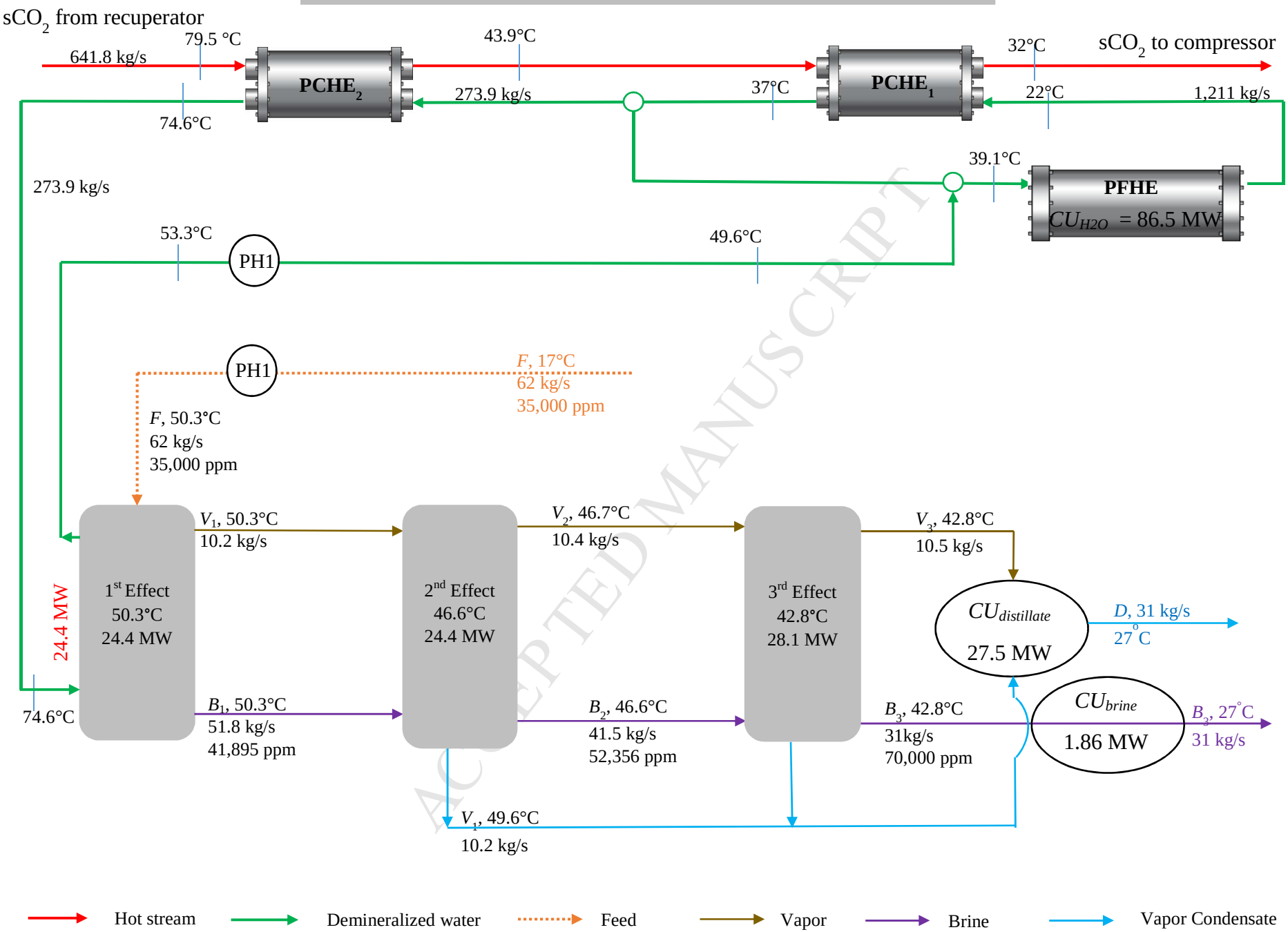

Fig. 9: Network for MED integrated with heated water, without sensible-heating evaporators 2B and 3B.

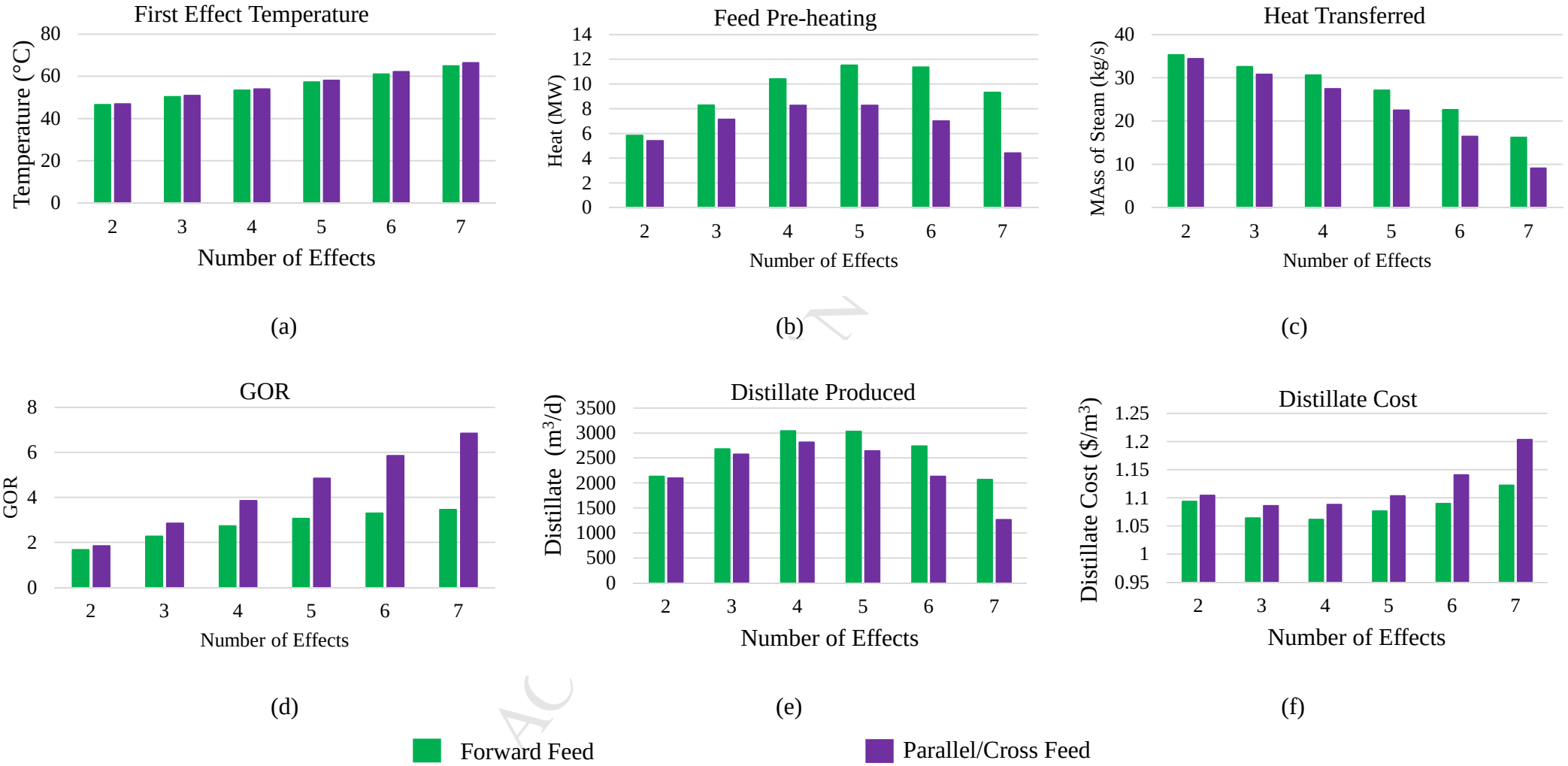

Fig. 10: Results for variation in number of MED effects on (a) the first effect operating (b) Feed pre-heating (c) net heat transferred (d) Gain output ratio (e) net distillate produced, and (f) distillate cost for forward and parallel/cross feed.

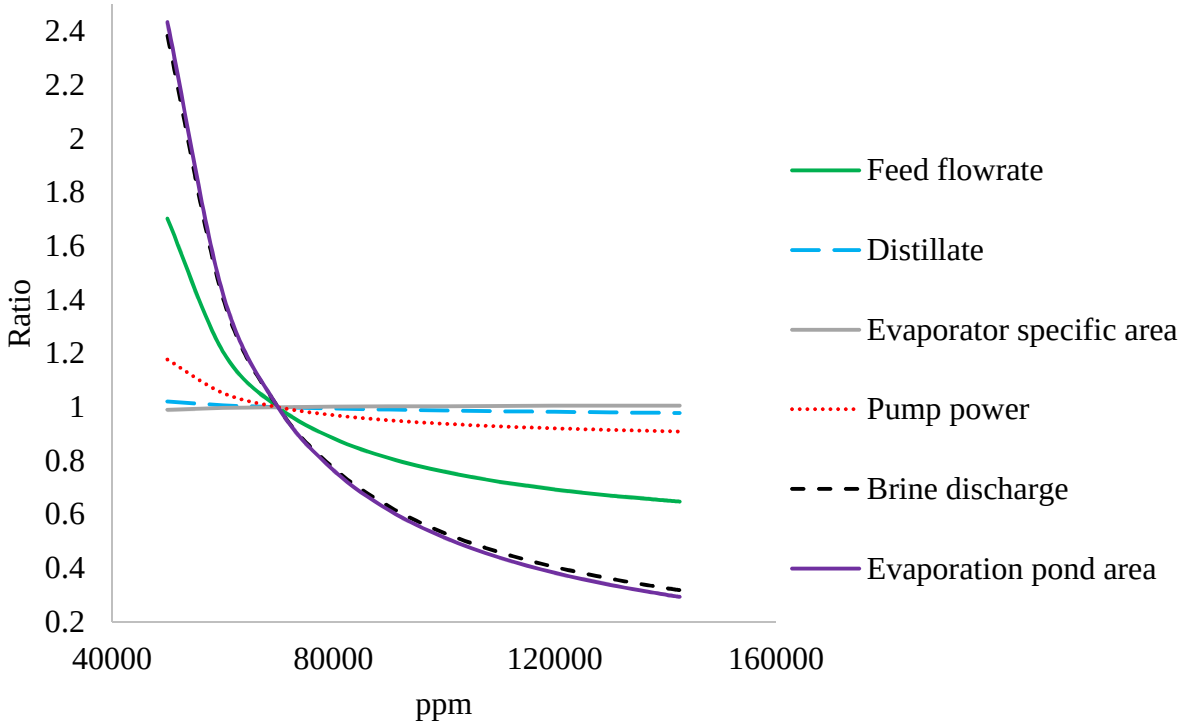

Fig. 11: Variation in MED performance with maximum brine concentration.

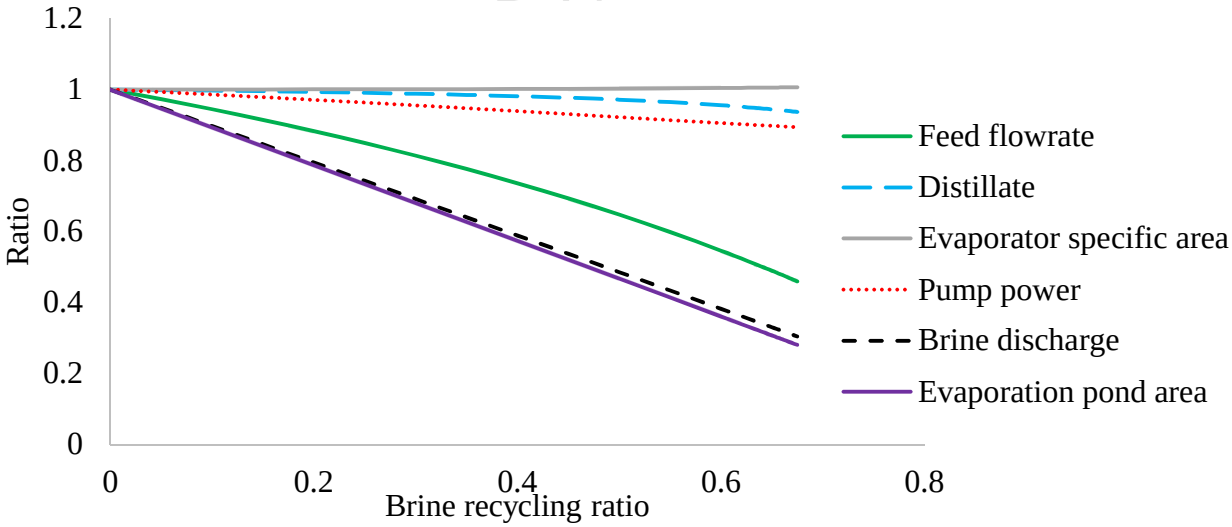

Fig. 12: Variation in MED performance with brine recycling.

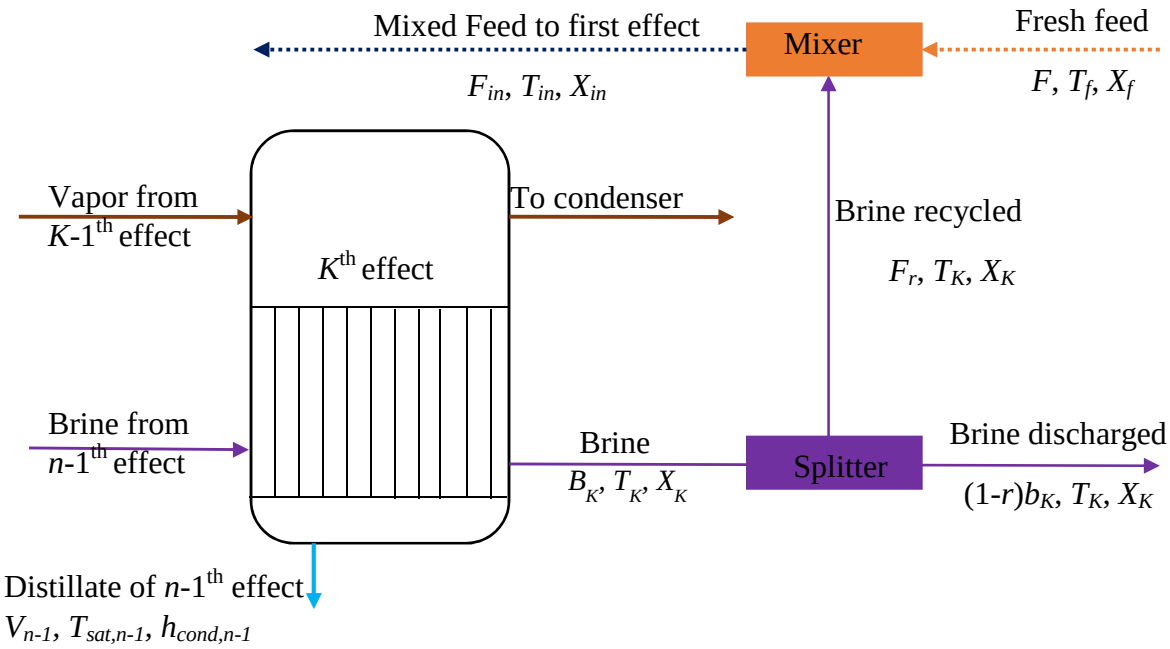

Fig. A1: Schematic for the brine recycling.

ACCEPTED MANU